

Thermal phenomena in MBBA*

Bojan Durickovic[†] Angus Hendrick[‡]

May 11, 2007

Abstract

We describe the phenomena observed in heating a thin film of MBBA from room temperature through the nematic-to-isotropic phase transition temperature, including color changes, bright and dark bands, nucleation and growth, and nematic-isotropic interface propagation. Plausible explanations are offered as to the underlying physical processes.

1 Introduction

MBBA (*p*-methoxybenzylidene-*p*-*n*-butylaniline¹) is a nematic liquid crystal at room temperature. At about 43°C, it undergoes a phase transition to an isotropic liquid [1]. The nematic-to-isotropic phase change is ‘weakly first order,’ in the sense that discontinuities are observed in the density, latent heat etc., however these discontinuities are small [2, 3].

In the isotropic phase, MBBA has no long-range order present. In the nematic phase, the rod-like molecules of MBBA align locally such that in a small volume (though large relative to the scale of the molecules) they possess an average orientation (i.e. directional order). This average orientation is termed the *director*. Translational order, however, is not present in nematic MBBA.

1.1 Optical birefringence

The director in a nematic liquid crystal defines an optical axis. Electromagnetic radiation propagating along this axis is subject to a single permittivity (ϵ) value regardless of its polarization. A different permittivity is experienced by light that is polarized parallel to the optical axis. For light not polarized normal or parallel to the optical axis, both permittivities are experienced, in other words, nematic liquid crystals are *birefringent*.

*Prepared for the final project in the Applied Math Laboratory (Math 697B), Spring 2007, Professor Michael Tabor.

[†]E-mail: bojan@math.arizona.edu

[‡]E-mail: angus.hendrick@gmail.com

¹line-notation: CH₃-O-Ph-CH=N-Ph-C₄H₉

1.1.1 Polarization effects of birefringence

For the purposes of this study, the most important consequence of birefringence in MBBA is that the polarization of transmitted light may be altered with respect to the polarization of the incident light. The polarization is altered when light that is not polarized normal to the optical axis is effectively broken into two components that travel at different speeds. When the two components exit the material and recombine, they have traveled for different times in the material. Since they have the same frequency, the phase relationship between the oscillating fields in the two components can be altered, which implies a change in polarization with respect to the incident light.

More specifically, the optical path length through a material is given by:

$$\text{OPL} = nd, \tag{1}$$

where n is the index of refraction ($n = \sqrt{\epsilon}$), and d is the physical distance traveled (sample thickness). A nematic liquid crystal, being birefringent, has two different indices of refraction, which we label n_o (for polarization normal to the optical axis), and n_e (for polarization parallel to it).² (In MBBA, $n_o = 1.8062$ and $n_e = 1.5616$ [4].) For incident light that is linearly polarized at a certain angle with respect to the optical axis, the components parallel and perpendicular to the axis will have travelled different optical path lengths over the same physical length, and the two will differ by the optical path difference

$$\text{OPD} = (n_o - n_e)d. \tag{2}$$

This optical path difference translates into a phase difference between the two components, generally giving an elliptical polarization (unless the phase difference is a multiple of $\pi/2$).

Crossed polarizers with an isotropic media between them do not allow any light to pass through. Thus, isotropic MBBA appears black when viewed in this fashion. Because nematic MBBA can alter the polarization of incident linearly polarized light to elliptical, placing it between perpendicularly oriented polarizers allows some light to be transmitted. This provides a ready method for visually distinguishing the nematic and isotropic phases of MBBA.

1.1.2 Color effects of birefringence

If the optical phase difference is a multiple of the wavelength, polarization will not be altered, and light will not be transmitted through the analyzer. For nearby wavelengths, light is elliptically polarized, but the field is rotated only through a small angle over the sample thickness, so that a small fraction of the intensity will be transmitted. In this way, parts of the spectrum of the incident light will have their intensity reduced in the transmitted light more than other parts of the spectrum, producing coloration of incident white light.

²The subscripts “o” and “e” are for ordinary and extraordinary.

1.2 Equilibrium phases

In simple thermodynamic terms, at any temperature the Gibbs energy G of the nematic and isotropic phases, respectively, may be considered as:

$$G_N = H_N - TS_N, \quad G_I = H_I - TS_I, \quad (3)$$

where T is temperature H is specific enthalpy, and S is specific entropy. H and S can be treated as constants for each phase.³ At constant pressure, the system will minimize its Gibbs energy at equilibrium. Thus at equilibrium whichever phase has the lesser Gibbs energy at a given temperature is the one that will be observed [5].

For MBBA, the situation can be understood as follows. The nematic phase is more ordered than the isotropic phase, and so has less specific entropy. Conversely, the alignment in the nematic phase allows for more molecular interactions (i.e. along the entire length of each molecule), which will tend to reduce the specific enthalpy. At low temperatures the nematic phase is stable due to its more negative enthalpy. As temperature increases, the larger entropy of the isotropic phase eventually results in it having the lower Gibbs energy. The temperature at which this occurs is the critical temperature for the phase change. If temperature is not uniform in the sample, both phases can be observed side by side, where the nematic-isotropic interface is the isothermal line⁴ at the critical temperature.

1.3 Phase nucleation and growth

In a perfectly pure and homogenous liquid crystal with an applied temperature gradient, the nematic-isotropic interface is located at the isothermal line corresponding to the critical temperature. The entire region on the warmer side is isotropic, and the region on the cooler side is nematic. In reality, impurities and defects can alter this simple picture.

1.3.1 Effect of defects

Lansac et al. [6] conducted experiments showing that nucleation of isotropic droplets in a nematic phase occurs at defects. One explanation for the appearance of isotropic phase within the nematic phase below the normal critical temperature is that defects in the director field increase the local energy of the nematic phase sufficiently to depress the local nematic-to-isotropic transition temperature. The following discussion follows from the work of Cermelli et al. [7].

The free energy difference $\widehat{\Psi}$ between the nematic and isotropic phases is

³This is true near the critical temperature.

⁴Actually, it is an isothermal surface in three dimensions, but the thickness dimension cannot be observed directly.

given by:

$$\hat{\Psi}(\mathbf{n}, \nabla \mathbf{n}) = \Psi_0(T) + \frac{k_1}{2}(\nabla \cdot \mathbf{n})^2 + \frac{k_2}{2}(\mathbf{n} \cdot \nabla \times \mathbf{n})^2 + \frac{k_3}{2}(\mathbf{n} \times \nabla \times \mathbf{n})^2 + \frac{k_2 + k_4}{2}((\nabla \mathbf{n})^2 - \nabla \cdot \mathbf{n}^2), \quad (4)$$

where \mathbf{n} is the the director, T is temperature, k_1, k_2, k_3 , and k_4 are the splay, twist, bend, and saddle-splay moduli, respectively, and Ψ_0 is termed the ‘‘ambient free-energy difference’’, and captures the effect of temperature on the free energy difference between the phases.⁵

In a defect-free material, the configurational energy terms (i.e. all terms depending on \mathbf{n}) are 0 and the free energy difference is governed solely by Ψ_0 , which is a function of temperature. At low temperatures, Ψ_0 is negative and the nematic phase is stable. At high temperatures Ψ_0 is positive and the isotropic phase is stable. At the critical temperature Ψ_0 is zero and the two phases may coexist.

The presence of defects causes the configurational energy terms to become positive. Thus $\hat{\Psi}$ will be greater than 0 before Ψ_0 reaches zero, and the material will transform to the isotropic phase below the critical temperature. For the special case of a director field oriented radially outward, a critical radius for a spherical droplet is given by:

$$R_* = \left(\sqrt{1 + \frac{\kappa |\Psi_0|}{\sigma^2}} - 1 \right) \frac{\sigma}{|\Psi_0|}, \quad (5)$$

where σ is the surface tension between the nematic and isotropic phases, and $\kappa = 2k_1 - (k_2 + k_4)$. This result reflects a balance between the force of the surface tension, which favors shrinking the drop to reduce the surface energy, and the force of the distortion, which favors increasing the size of the drop to reduce the amount of the distortion energy. These forces are constants of the defect and material, so the equilibrium radius varies with the ambient free-energy difference Ψ_0 and thus temperature.

The formula predicts an equilibrium value of R_* for all values of Ψ_0 . As a practical matter, the equilibrium value of R_* is only relevant where the nematic phase is stable (i.e. $\Psi_0 < 0$), as otherwise the material transforms entirely to the isotropic phase. Using characteristic values of the parameters ($\kappa = 10^{-7}$ ergs/cm, $\sigma = 10^{-2}$ ergs/cm²), Cermelli et al. estimate that near the critical temperature (i.e. $\Psi_0 \lesssim 0$), $R_* \approx 10^{-1}$ μ m. For lower temperatures, the drop will be smaller.

1.3.2 Effect of impurities

Introduction of impurities into a pure substance reduces the temperature at which the nematic-to-isotropic phase change occurs. Returning to equation (3),

⁵ Ψ is akin to the Landau energy, a coarse-grained Gibbs energy.

intuitively this is because impurities disrupt ordering, reducing the enthalpic contributions in the ordered nematic phase.

More formally, the Gibbs energy of each phase is a function of the concentration of the impurity:

$$G = H_0 + H(C) - T(S_0 + S(C)), \quad (6)$$

where C is the concentration of the impurity. Here H_0 and S_0 are the specific enthalpy and entropy of the pure phase, and $H(C)$ and $S(C)$ are the compositional dependence of these quantities. For physical reasons we expect:

$$\frac{\partial H}{\partial C} > 0, \text{ and } \frac{\partial S}{\partial C} > 0. \quad (7)$$

That is, impurity increases the enthalpy of the phase by reducing the bonding, and it increases the entropy by creating more possible arrangements of the atoms.⁶ Thus, at a given temperature, a plot of the Gibbs energy of the two phases as a function of concentration might appear as shown in Figure 1. In

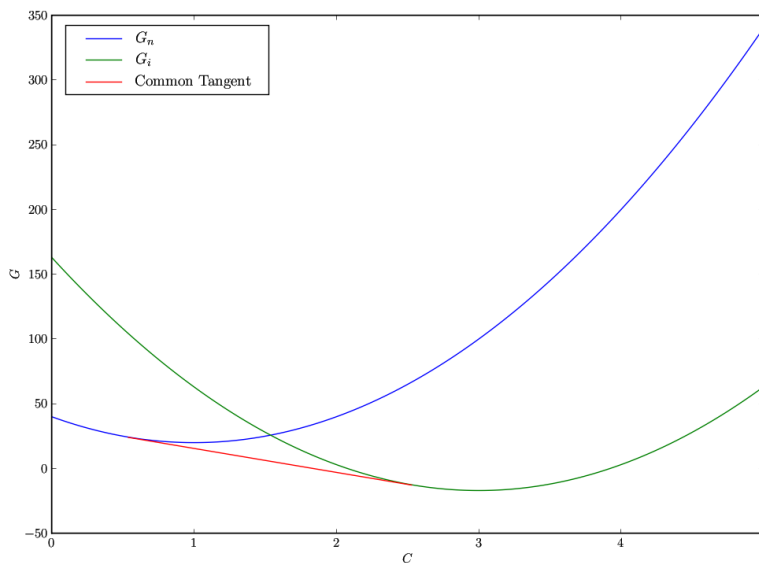


Figure 1: Notional depiction of Gibbs energy for nematic and isotropic phases with impurities present near the critical temperature. Arbitrary units.

the region of impurity concentrations where the common tangent construction is shown, the material can lower its Gibbs energy by separating into two phases

⁶We assume that the impurity does not form a compound with the pure material, and that the concentration is less than 0.5.

with differing concentrations of impurity. The nematic phase will be depleted in the impurity, while the isotropic phase will be enriched in it. Assuming that the concentration profile is initially uniform, the segregation of the impurity between the phases will require diffusion in the nematic to the interface.

1.4 Natural convection

Liquid crystals are susceptible natural convection in a fashion similar to other liquids. Though the viscosity of nematic MBBA is a tensor property, this is neglected for simplicity to emphasize the factors that govern the phenomenon.

1.4.1 Rayleigh-Benard instability

In a fluid heated from below, a temperature gradient is developed in the vertical direction. Because the fluid density decreases with increasing temperature, the warmer lower portion of the fluid feels a rising force while the cooler upper portion feels a falling force. These forces coupled with the continuous introduction and removal of heat at the bottom and top of the fluid can lead to steady flow of the fluid in circular fashion termed convective rolls, wherein multiple small cells of fluid roll about axes parallel to the top and bottom surfaces, and neighboring cells rotate in opposite directions.

The characteristic number for the onset of this instability is the Rayleigh number,

$$\text{Ra} = \frac{\Delta T \alpha g h^3}{\kappa \nu}, \quad (8)$$

where ΔT is the temperature difference from top to bottom, α is the thermal expansion coefficient, g is the gravitational acceleration, h is the height of the cell, κ is the thermal diffusivity, and ν is the kinematic viscosity. Development of natural convection between two plates typically results when $\text{Ra} > 1706$ [8].

1.4.2 Optical effects of natural convection

The onset of natural convection and the resulting thermal rolls causes optical effects in a nematic liquid crystal. The effects are described in detail by Penz [9], and Kramer et al. [8]. In essence the regular rolls of convecting fluid create periodic disturbances in the director field. These disturbances cause periodic variations in the optical axis. The shifting optical axis causes periodic focusing and defocusing of light, which then appears as light and dark bands.

2 Methods

The experimental setup, comprising a temperature control system and an optical system, is depicted in Figure 2. The schematic of the part of the setup holding and controlling the sample is shown in Figure 3.

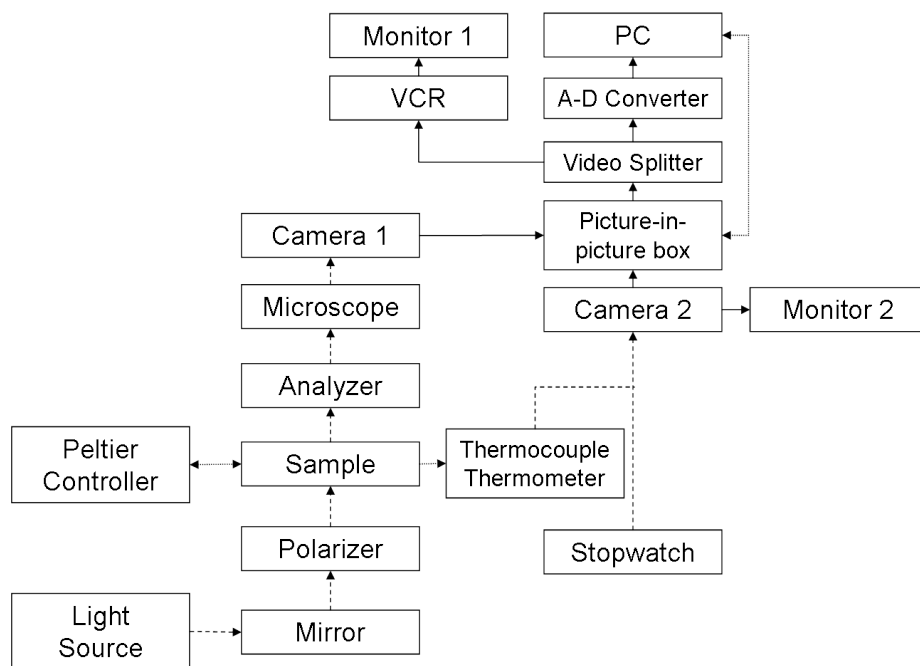


Figure 2: Hardware Schematic. Solid lines indicate video signal flow. Dashed lines are optical paths. Dotted lines are controller connections. The Sample block is shown in detail in Figure 3.

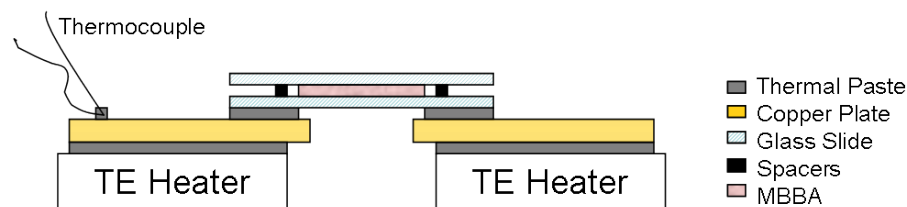


Figure 3: Schematic side view of the sample.

2.1 Sample preparation

A sample of 3–4 μ l of liquid MBBA was placed between two microscope slides⁷ separated by 13 μ m thick spacers.^{8–9} The bottom slide was positioned on top of a copper plate with a circular hole 6.35mm in diameter (hereinafter termed the *optical* or *viewing window*) in the center. The thermal conduction at the

⁷With the exception of a few samples where alternative assemblies were tried, both slides were 0.17–0.25mm thick (Fisher Scientific Co., Cat. No. 12-543C).

⁸Shim Stock, manufactured by Artus Corporation, Englewood, NJ. The nominal spacers thickness was 0.0005”.

⁹Some practical issues with sample thickness are discussed in Appendix B.3.

contact between the slide and the copper plate was facilitated by a layer of thermal compound¹⁰. The thermal compound was not applied to the entire area of overlap of the slide and the copper plate. An annulus around the optical window was not covered in an effort to avoid introducing thermal paste into the viewing window. We will refer to the area where the slide was not in contact with thermal paste as the *thermal window*.¹¹

The copper plate was positioned atop two Peltier thermoelectric devices (henceforth: TE devices) so that the optical window was unobstructed between them. The contact between the copper plate and the TE devices was coated with the same thermal compound as the one with the slide. The entire stack was then covered by a piece of insulation with a hole in it to allow the microscope optics to view the sample through the viewing window.

2.2 Temperature control system

The two TE devices were connected to the same feedback controller, which allowed positive control over the temperature difference between the top and bottom of the TE device.

The bottoms of the TE devices were mounted to an aluminum base plate which acted as a heat source or sink. The base plate contained channels through which was pumped a liquid from a large reservoir. The large reservoir of fluid provided a relatively stable thermal foundation for the bottom surface of the TE devices, and by varying the current to the TE devices it was possible to obtain a desired temperature at their top surface.

This temperature was measured with a K-type thermocouple affixed to the top of the copper plate by thermal paste and a piece of cellophane tape. The accuracy of the thermometer was 1°C. However, the precision appeared to be closer to 0.1°C, based on the repeatability of temperature measurements. The precision of the temperature measurements and the temperature control system provided control over the temperature well within that precision in the temperature range in which the measurements were carried out (20–50°C).

2.3 Optical system

The optical system consisted of a light source¹², mutually perpendicular polarizer and analyzer, a microscope with magnification 10x or 25x, and a camera. In order to minimize the effect of the heat from the light source, the latter was separated from the microscope by a glass wall, and light was reflected on a mirror by 90° into the vertical optical axis passing through (in this order): the polarizer, the sample, the microscope objective, the analyzer and the camera objective.¹³

¹⁰Thermal Compound, part no. 120-8, Wakefield Engineering Inc, Beverly, MA.

¹¹See Appendix B.1 for a discussion on this and other thermal conditions.

¹²DYNA LITE 150 Fiber Optic Power Supply, A.G. Heinze Precision Microoptics

¹³Some practical issues with the optical system setup are discussed in Appendix B.2.

2.4 Image capturing and processing

The output of the camera was connected both to a VCR input and to a PC computer through a graphic interface card¹⁴. A second camera captured the displays of the thermometer and a stopwatch. A picture-in-picture capability permitted including this output into the captured frame of the sample.

Images were captured in 24-bit color at 640x480 resolution into an uncompressed TIFF format based on an assessment that this was the highest quality image that did not contain artifacts from up-sampling. The capturing process was alternately geared toward one of two approaches: focusing on a fixed region over time as the temperature changed (both on VCR and PC), and panoramic shots of the sample at steady-state. The panoramas of the sample at equilibrium were assembled by manual and automatic generation and matching of neighboring images using the software packages `generatekeys`, `autopano`, and `hugin`. The images were then stitched with the software package `nona` and then blended with `enblend`.¹⁵ To avoid distorting the images, the camera lens was modeled as cylindrical, and a cylindrical projection was used.

2.5 Analysis

The panoramic pictures of the optical window were analyzed using an image analysis and processing software capable of performing a variety of measurements and modifications to images.¹⁶

3 Observations and results

Several samples of MBBA were heated from the nematic room temperature phase through the isotropic phase change at about 43°C. Close to the critical temperature, the sample in the (cooler) center of the viewing window was in the nematic phase, while the region near the (hotter) periphery was isotropic, having undergone the phase transition. Near the interface between the phases, various phenomena were observed, which are broadly classified as static or dynamic, depending on whether the sample was in steady-state or local temperatures were changing.

Because analyzing high temporal resolution images was difficult—requiring first video taping the process and then replaying the video frame by frame to capture individual images—only descriptive observations of dynamic phenomena are offered. Some of the static phenomena were analyzed in detail by measuring features on panoramic images of the sample.

¹⁴Snappy Capture Device and Snappy Capture Software, made by Play, Inc. Some comments about the software are noted in Appendix B.4.

¹⁵These packages are available at <http://hugin.sourceforge.net/>

¹⁶ImageJ (Image Processing and Analysis in Java). Web site: <http://rsb.info.nih.gov/ij/>.

3.1 Static features

3.1.1 Mechanical compression

A freshly assembled sample where the top slide was gently rested (without compression) on top of the MBBA and spacers showed no coloration. Its optical properties did allow for the light to pass through the crossed polarizers, but all the observable features were varying intensities of white light (i.e. shades of gray). When the sample was compressed¹⁷ (still at room temperature), the gray landscape turned into vivid colors (see Figure 4).

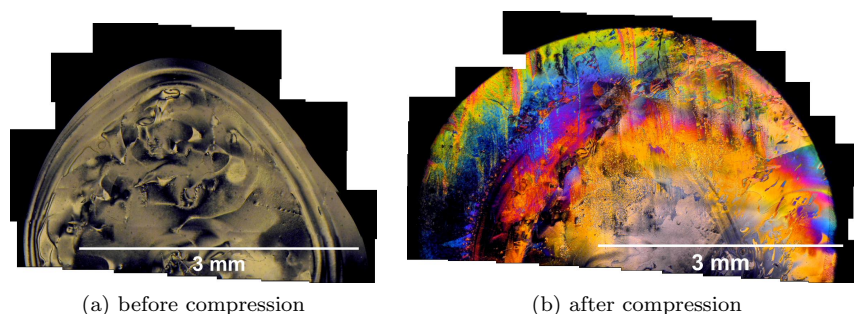


Figure 4: Effect of mechanical compression on the MBBA sample. (a) The entire sample was visible in the viewing window. (b) The sample spread out beyond the edge of the viewing window; coloration. Both pictures were taken at room temperature; the sample was not heated since assembly.

3.1.2 Varying sample thickness

The fact that some of effects observed during heating appear to depend on sample thickness led us to a side investigation of the effect of changing thickness below the spacers thickness.

A sample was prepared with a spacer on one side and the top and bottom slides in contact on the other side¹⁸ to form a wedge in the vertical direction. This allowed observation of gradual property changes in terms of sample thickness. Toward the thinner side, the sample showed no coloration and appeared gray.

3.1.3 Temperature gradient

At steady-state conditions above room temperature, a (horizontal) temperature gradient in the viewing window was present. This gradient resulted from

¹⁷The first time, this was done accidentally by pressing the microscope objective against the glass slide. Taught by this experience, we devised a way of compressing the samples in a consistent way, described in Appendix B.3.

¹⁸We are grateful to Prof. Robert Erdmann for the suggestion.

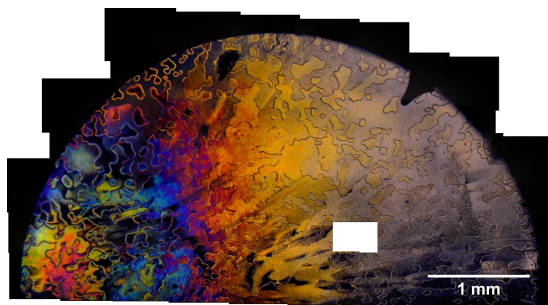


Figure 5: Sample with an inclined top slide. Thickness is $12\mu\text{m}$ at the left edge and $7\mu\text{m}$ at the right edge of the visible area. The panorama was taken at $T = 41.8^\circ\text{C}$, below phase transition temperature.

the simultaneous conductive perimeter heating and convective heat loss to the surroundings through the top and bottom surfaces of the glass window. Temperature measurements were carried out (with no MBBA sample present) by placing one thermocouple at the edge and another at the center of the viewing window, recording the temperature difference at various temperatures in the range from the room temperature to above the critical temperature.

The temperature profile of the viewing window was estimated (assuming axial symmetry) by solving the heat equation for a disk with a constant temperature boundary condition over its edge and heat loss to the surroundings over its surface, and then fitting this solution to the measured temperatures at the edge and at the center of the viewing window (see details in Appendix A). The resulting temperature profile estimate is shown in Figure 6.

Near the critical temperature, the temperature gradient allowed observation of the nematic and isotropic phases and the interface between them in static (or quasi-static) conditions, as well as front propagation in non-static conditions.

3.2 Dynamic phenomena

Unless otherwise noted, the phenomena below were observed in all samples.

3.2.1 Gradual color changing

As the samples were heated from room temperature to about 1°C from the critical temperature, there was no apparent change in the patterns observed at room temperature except gradual changes of color, preserving the overall shapes of the features. A region of a sample is shown at three different times during heating in Figure 7.

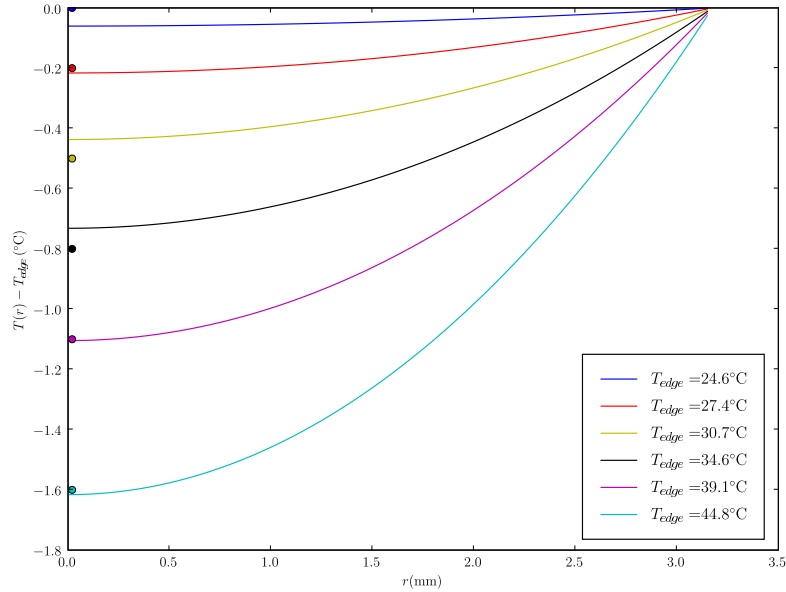


Figure 6: Estimated temperature profile in the viewing window (6.35mm diameter) plate at various edge temperature and 23°C ambient temperature. Circles indicate measured values at the center.

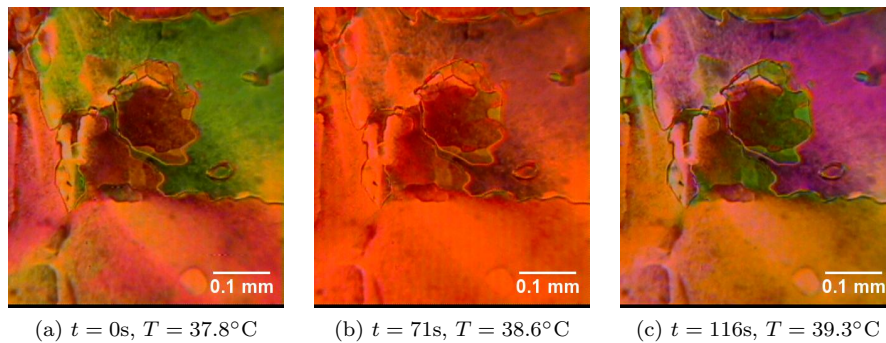


Figure 7: Gradual change of color. The phase transition temperature was above 40°C.

3.2.2 Color changing front

In some samples, a front would sweep the sample from the edge inwards discontinuously changing the color.

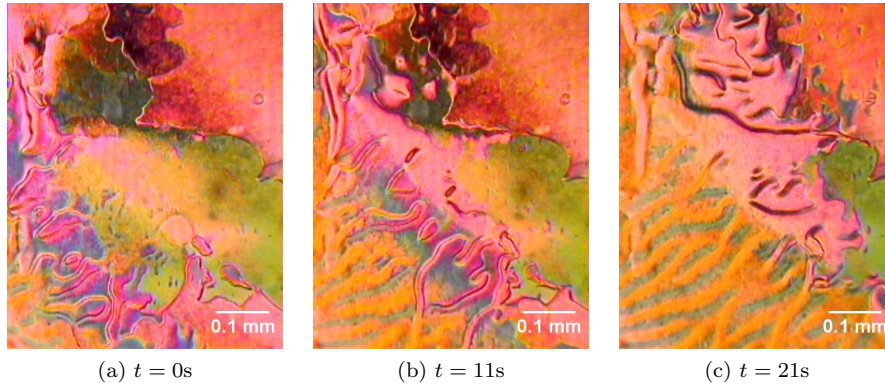


Figure 8: Color changing front, followed by the the bright and dark bands that eventually tend to orient themselves along the front propagation direction. $T = 38.3^\circ\text{C}$. The sample is the same one as in Figure 7.

3.2.3 Bright and dark lines

The color changing front was almost always followed by the appearance of bright and dark lines, that would gradually orient themselves parallel to each other. In one sample that exhibited this behavior, the lines did not follow the front immediately, so that the front initially had no other visible effect than to change the color of the sample, not affecting the patterns. In another sample (shown in Figure 8), the lines followed the front immediately, making the patterns previously present in the sample difficult to identify.

3.2.4 Brushing front

In one sample, rather than having a color changing front that would leave the overall patterns in the sample intact, a front was observed that swept the sample with a more dramatic impact, shown in Figure 9. The front itself was black and about $50\mu\text{m}$ wide, and was leaving behind it a black and white sea of defects and brushes, erasing all patterns and colors.

3.2.5 Nucleation, growth and coalescence

When the temperature reaches about $0.1\text{--}0.2^\circ\text{C}$ below the phase transition temperature, nucleation of small bright “droplets” starts. Due to the approximately axial symmetry of the temperature profile, regions where nucleation would occur at a given time were of ring-like shape. When the droplets reach a certain size (which may depend on the heating rate, temperature gradient and other factors; the observed ones were up to $30\mu\text{m}$ wide), they turn black and start growing faster. As they grow into each other, they coalesce into larger droplets, changing shape so as to distribute the curvature more evenly (i.e. tending towards a

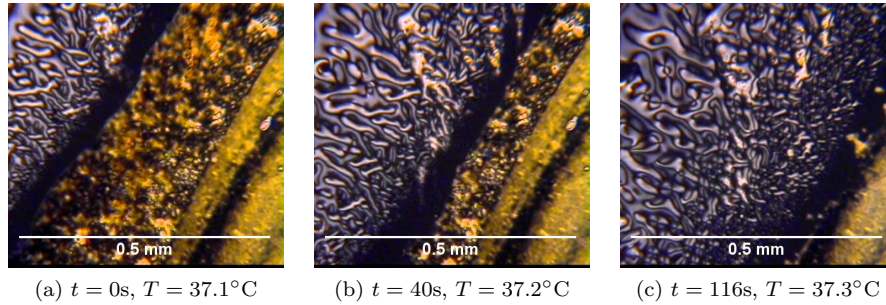


Figure 9: “Brushing front.” The sample is the same as the one in Figure 4.

circular shape).

This phenomenon was the most commonly observed one. Every sample exhibited this behavior, with varying density of nucleation and growth speed. In some cases, the initial phase of bright droplets was hard to observe, as the droplets would turn black at a very small radius.

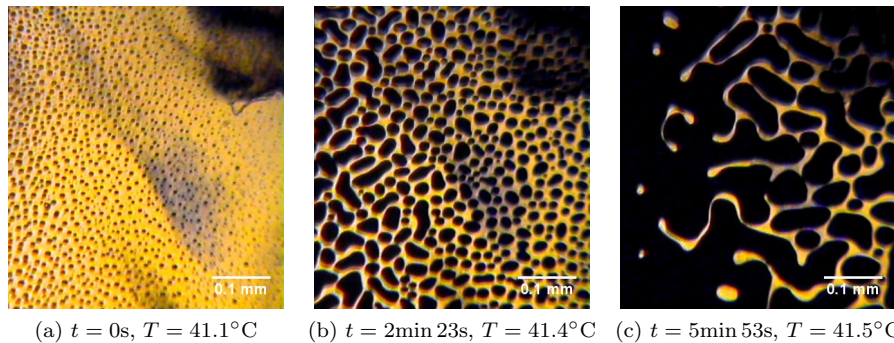


Figure 10: Nucleation, growth, coalescence and encroachment. In each picture, the temperature is decreasing from left to right. (a) Isotropic droplets nucleate and grow. (b) Smaller droplets coalesce into larger ones. (c) Eventually they coalesce with the bulk isotropic region, visible here in the left part of the picture. The bulk interface propagates to the right.

Steady state Growth would stop if temperature was brought to a steady state. Thus, we were able to observe a static equilibrium distribution of nucleated droplets and bulk interface. One such configuration is shown in Figure 11.

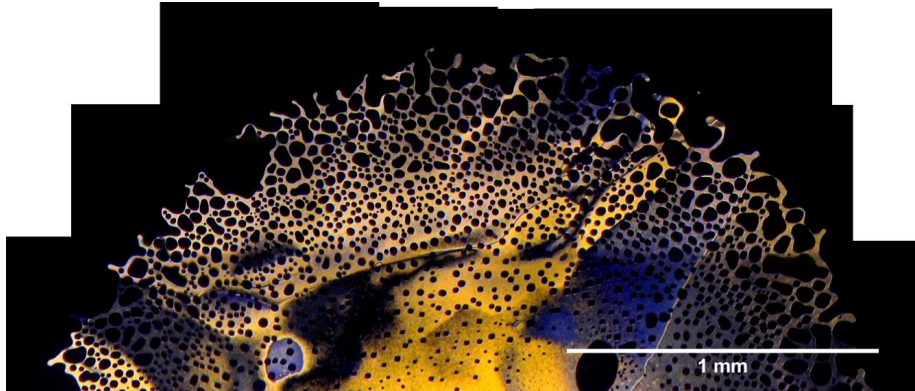


Figure 11: Static configuration of nucleated droplets and bulk interface. Observe that as we look at the regions from the (relatively cold) center towards the (relatively warm) edges, a progressively larger fraction of the area is covered by the isotropic phase.

3.2.6 Encroachment

Provided that the heating rate was slow enough, the droplets nucleated at about the same time would coalesce both with each other and with a bulk black region formed by droplets nucleated before them that had already coalesced into a uniform, connected region, extending from a given radius to the edge of the viewing window (see Figure 10c). This connected region is henceforth referred to as the *bulk isotropic phase*.¹⁹ Then a single interface curve between the bulk isotropic phase and the nematic phase in the center could be identified. This interface (which may be called the “bulk interface”) would propagate inwards as the sample is heated, invading the nematic phase both by growing and by coalescing with isotropic droplets nucleated inside the nematic phase.

4 Discussion

4.1 Sample thickness

4.1.1 Mechanical compression

Comparing the non-compressed and the compressed sample shown in Figure 4, the area covered by the sample is increased after compression. Since the volume is constant, the thickness of the sample was decreased. Apparently, the weight of the top slide is not sufficient to press the sample down to the thickness of the spacers, presumably because the surface tension is sufficient to resist the weight of the relatively light top slide.

¹⁹If the sample is heated rapidly, droplets start nucleating throughout the sample before the ones along the edge of the viewing window had time to coalesce completely.

4.1.2 Gray samples

Gray samples (i.e. no coloration) were observed both in the thin (Figure 5) and thick (Figure 4) limit.

In the case of the sample with the inclined top slide, the gray region extended to a thickness of about $7\mu\text{m}$. At this thickness the optical path length difference (2) is about

$$\text{OPD} = (1.8062 - 1.5616)7\mu\text{m} = 1.7\mu\text{m}.$$

This is roughly 2–3 wavelengths of visible light ($\lambda = 400\text{--}700\text{nm}$), and much larger than the wavelength difference between the ends of the spectrum. On the face this should be sufficient to cause color dispersion, However in the above calculations it was implicitly assumed that the director field is homogenous throughout the thickness of the sample.

It is reasonable to assume that when the MBBA droplet is first placed on the slide, it has a director field that varies widely over space. This makes it appear gray, because birefringent effects are spatially averaged such that some amount of all wavelengths is able to pass through any region of the top surface that is small enough to discern with the microscope. Flow of the sample can act to align the director field through the action of shear forces on the director field. Greater spatial correlations of the director field will give rise to discrete wavelength cancellations over visible regions, making them appear colored.

In the case of the thick sample, it is suggested that when the sample was compressed the induced flow caused alignment of the director field over larger regions of space, eliminating the averaging and causing colors to appear. This is consistent with Figure 4, to the extent that the center, where flow would be least is still relatively gray compared to the more colorful edges. Similarly, the wedge sample is believed to be grey on the thin side because that fluid did not flow during sample construction, whereas the thicker section of fluid was driven there by the placement of the top slide. This would cause director field alignment and color.

4.2 Brushing front

As the sample shown in Figure 9 was assembled in a very similar fashion to later samples which showed consistent behavior and no such phenomena, we attribute the unique behavior in this sample to the fact that it was severely pressed (accidentally, before the heating, by the microscope objective). This may have introduced a large number of defects observed among the brushes after the front. Only one other sample exhibited this behavior (the one shown in Figure 5), in which defects were observable below the critical temperature.

4.3 Encroachment

Modeling of the kinetics of the nematic-isotropic interface is a problem that has received considerable attention from theorists [7, 10, 11, 12]. These models assume a (macroscopically) ordered (either radial or uniform) director field and do

not take into account defects, nucleation and coalescence. However, coalescence with nucleated droplets constituted the dominant mode of interface propagation in our samples. Moreover, even though the temperature profile is not expected to deviate significantly from a circularly symmetric profile, the actual boundary between the bulk isotropic material and the nematic material is not circular, but has considerably more structure. The fact that the bulk interface does not follow the critical temperature isotherm can be attributed to the coalescence with nucleated isotropic droplets inside the nematic phase.

4.4 Nucleation and growth

Cermelli et al. [7] developed a model for the nematic-isotropic interface propagation (cf. Section 1.3.1 above) yielding a simple formula for the stationary radius of curvature of the interface, that we could compare with our measurements. However, this radius is submicroscopic ($0.1\mu\text{m}$), and is much smaller than the radii of stable droplets observed at constant temperature in our experiments (cf. e.g. Figure 11). In order to explain what we observed, we invoke the effect of impurities presented in Section 1.3.2.

In the model proposed by Cermelli et al., the ambient free-energy difference Ψ_0 is primarily taken to be a function of temperature. It is noted, however, that Ψ_0 could also account for variations as a result of concentration variation. We note that “pure” MBBA may be only 99% MBBA (i.e. 1% impurities) [1]. Furthermore, the handling required to construct samples can introduce further impurities.

The following behavior is suggested. Initially, sub-microscopic cells of isotropic phase exist in the nematic phase as a result of defects. As the temperature increases, these cells grow slightly but remain submicroscopic. As the Gibbs energy of the isotropic phase falls due to the increasing temperature, the material enters the region where the system can lower its Gibbs energy by separating into phases of different concentrations. Before this can occur, impurity must diffuse into the isotropic phase. Initially, this is a slow process, because the isotropic cells are small and the impurity must diffuse a long distance. Thus the isotropic cells grow slowly. However, as they grow, the diffusion distances become shorter, and so they grow faster and faster until the material reaches an equilibrium in which the nematic and isotropic phases exist at the endpoints of the common tangent construction. This rapid growth can happen at nearly constant temperature. However once the material reaches this equilibrium, the growth slows down and is controlled by the shifts in the endpoints of the tangents resulting from the effect of continued temperature changes.

4.5 Conclusion and further work

Our experimental setup allowed us to observe a wide range of phenomena, some of which depended strongly on the details of sample assembly and thickness, and possibly on the heating rate, vertical temperature gradient and other parameters. The phenomena observed were not always consistent with our preconceived

intuition based on simplified theoretical models, and we attempted to provide plausible arguments to reconcile these models with a real system containing impurities.

In our experiments, we did not have complete control over some parameters, such as the vertical temperature gradient, and director anchoring at the glass slides. Controlling these is crucial for a more complete understanding of the observed phenomena and for comparison of possible models with experiments.

Two phenomena that we observed caught our attention in particular: the appearance of bright and dark lines just below the phase transition, which occurred in some samples only, and the nucleation of isotropic droplets below the nominal critical temperature, which was observed in every sample. In this paper, we offered rather qualitative interpretations of these two phenomena.

As for the bright and dark lines, their appearance, in our view, should depend strongly on the sample thickness and to a lesser degree on the vertical temperature difference (the critical number is $Ra \propto \Delta T h^3$). Further experiments, where the vertical temperature difference would be measured (e.g. using the technique described by Marinov and Simova [13]) and with varying and controlled thicknesses would confirm or disprove our hypothesis of Rayleigh-Benard convection rolls.

The descriptive model of nucleation of isotropic droplets in a liquid crystal with impurities presented in this paper (Section 4.4) could be tested by developing the model further and comparing of the observed experiments with numerical simulations.

Appendices

A Thermal analysis

Because the phenomena of interest are dependent upon temperature, a thermal analysis was performed to estimate the temperature profile in the viewing window based on the temperature measured at the thermocouple on the copper backing plate. The convenient location for measuring the temperature during the experiment is remote from the viewing window, near the edge of the copper plate. Consequently, between the sensing thermocouple and the edge of the viewing window, there was a relatively large (compared to the viewing window) conducting stack comprising the copper plate, thermal paste, and the glass slide. Simultaneous temperature measurements were taken at the edge of the viewing window and the normal sensing location. Figure 12 shows the temperature data and the best fit line. This correlation was used to estimate the temperature at the edge of the viewing window from the sensing temperature. Because the thermal conductivity of copper (401W/(mK)) is very high relative to the glass slide (1.1W/(mK)), it was assumed that the temperature around the perimeter of the viewing window was uniform.

A steady-state model of the temperature in the viewing window was de-

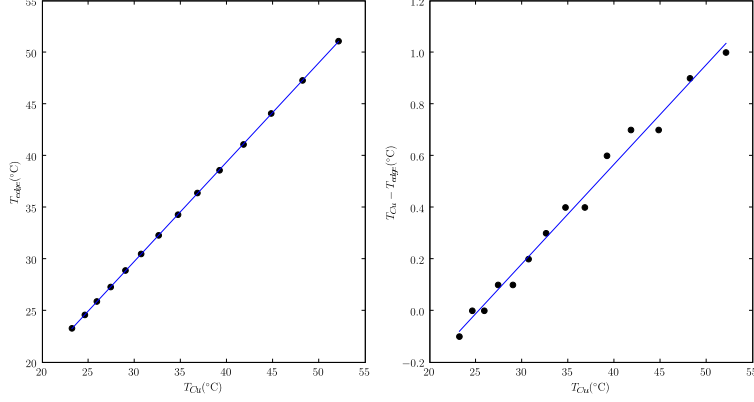


Figure 12: Indicated temperature versus viewing window temperature.

veloped. The window was modeled as a disk with a fixed temperature at its perimeter, with convective losses over its surface. The temperature T in the window area is governed by a Poisson equation with temperature dependent source term:

$$k\nabla^2 T = \frac{h}{t}(T - T_0), \quad (9)$$

where k is the thermal conductivity of the glass, h is an empirically determined heat transfer coefficient, t is the thickness of the glass plate, and T_0 is the ambient temperature.

We consider the system as radially symmetric. One boundary condition is given by a constant temperature at the edge of the domain (set by the temperature of the copper), and the other one by the smoothness at the origin.

$$T(r = R) = T_{\text{Cu}} \quad (10)$$

$$\left. \frac{\partial T}{\partial r} \right|_{r=0} = 0, \quad (11)$$

Expanding the laplacian operator in polar coordinates in equation (9) gives:

$$k \frac{1}{r} \frac{\partial}{\partial r} \left(r \frac{\partial T}{\partial r} \right) = \frac{h}{t}(T - T_0) \quad (12)$$

Now, solving equation (12) subject to boundary conditions (11) and (10) gives

$$T(r) = \frac{(T_{\text{Cu}} - T_0)I_0(ir\sqrt{\frac{h}{kt}}) + T_0I_0(iR\sqrt{\frac{h}{kt}})}{I_0(iR\sqrt{\frac{h}{kt}})}, \quad (13)$$

where I_0 is the 0th-order modified Bessel function of the first kind.

To fully specify the temperature, the heat transfer coefficient h must be determined. A variety of relations are reported by Khalifa [14]. Among those for horizontal discs oriented downward, the one that appears most applicable is

$$h = 1.065(T - T_0)^{0.27} \text{W}/(\text{m}^2\text{K}),$$

which is given for discs of up to 0.25m in diameter. Khalifa noted that actual heat transfer coefficients can vary by up to a factor of four. The given value was multiplied by 2.8 to match measured data for the laboratory configuration.²⁰ Figure 6 shows the temperature estimate of the model as compared to the data (taken only at the center). These profiles were used for assessing the local temperature when evaluating the various phenomena observed.

B Issues with the experimental setup

We present here several practical issues we were faced with in setting up and carrying out the experiment.

B.1 Thermal conditions

Establishing known and repeatable thermal conditions required care in several areas, and was important for making experiments both repeatable and measurable.

Thermal window Good thermal contact between the slide and the copper plate was only present where there was thermal paste. If the thermal paste did not reach (or extended past) the hole in the copper plate, then the optical and thermal windows²¹ were different, making the estimation of temperature within the viewing area more difficult. In our samples, the thermal window was roughly circular and about 2mm larger in radius than the optical window. Making the temperature profile repeatable depended strongly on the reproducibility of the thermal window, and (in our opinion to a lesser degree) on making the bottom slide stick uniformly to the thermal compound in the region of contact. The effect on the temperature profile was apparent from the shape of the outermost nematic–isotropic interface in some measurements, which—in some cases—was clearly non-circular. This was the result of the non-circular shape of the thermal window. The shape of this curve was hard to control, and the deviations were of the order of 1mm.

²⁰This factor may also be accounting for the fact that convection could be from both surfaces.

²¹By *thermal window* we mean the inner boundary of the region of contact between the glass slide and the thermal compound.

Microscope objective and thermal profile The distance between the top slide and microscope objective was not the same for the 10x and the 25x objective. This may have rendered the temperature profile of the snaps taken with the 25x objective incomparable with the one for the 10x objective (which was used for the vast majority of our observations), the reason being that the heat loss through the top slide may have been much smaller in the case of the 25x objective due to its close proximity to the top slide. We did not carry out temperature measurements for the 25x objective.

Rate of heating The relaxation time of the temperature control system near the critical temperature (around 43°C) was of the order of several minutes. It was important for our measurements to have conditions close to equilibrium when phase transformations started occurring, which means that we needed to become familiar with the response of the controller so as to avoid temperature overshoot.

Choice of microscope slides A thin bottom slide reduced both the thermal mass of the slide and the thickness of relatively low thermal conductivity material (glass) between the copper and the sample. This decreased the relaxation time between temperature changes on the TE units and temperature changes in the sample, reducing the risk of overshooting when establishing steady state conditions.

B.2 Optical issues

Automatic brightness adjustment This feature of the camera was turned off to allow better comparison among images with different overall brightnesses. The digital charge-coupled device (CCD) camera used to capture the images for these experiments was equipped with a feature that automatically adjusted the sensitivity of the camera based on the overall brightness of the image. This feature was on by default and was on during several initial experiments. As the nematic phase transitioned to isotropic, the field of view would become progressively darker, leading to the remaining nematic phase appearing brighter and brighter as the automatic sensitivity adjustment increased the gain. When the field of view was almost entirely isotropic (black), the remaining bits of nematic material would appear as over-saturated white. Turning this feature off eliminated this behavior and revealed that the brightness of smaller pockets of nematic phase was no more or less than large regions.

Color neutralization Though ultimately not critical for these experiments, obtaining images that accurately reflect the optical behavior of the sample required that the color be adjusted to neutral. Images were taken with red, green, and blue filters and then analyzed using ImageJ software to ensure that they were in fact red, green, and blue as captured by the computer.

B.3 Sample thickness

Establishing a standard sample thickness was found to be important to obtain repeatable results. For example, phenomena such as convective rolls and color depend on the thickness of the sample.

To obtain a sample of constant thickness, spacers of same thickness were used in all experiments. After placing the cover slide atop the sample and the spacers, a 500g flat-bottomed weight was then placed atop the cover slide such that it would compress the sample. The weight was wide enough that when the sample was compressed to the thickness of the spacers, the load would be transmitted through the cover slide directly to the spacers. Samples produced in this fashion were more consistent in the characteristics they displayed during heating than samples prepared without loading.

Attempts were also made to construct samples with a smaller vertical temperature gradient by using thermal paste between the spacers and the glass slides. However, this resulted in a more uncertain sample thickness, as the quantity and distribution of thermal paste on the spacers was difficult to control.

B.4 Snappy software

Two limitations of the Snappy Capture Software that were noted during the course of several experiments were

1. Snappy is not intended for fast image capturing. The fastest rate it allowed was a frame every 3 seconds. Phenomena occurring on time scales of a second or less were thus impossible to capture.
2. Snappy is not adapted for capturing and saving many frames in a sequence. Our panoramic snaps of the entire visible sample typically had about 100 frames, while in an experiment with a varying temperature we would take several hundred frames in a sequence. Each of these images had to be manually selected in a window which showed only four images in order to save it. Though the “Quicksave” feature would allow saving of all images once selected, the selection process was time-consuming. The white area in Figure 5 is most probably a result of an image that was inadvertently not saved.

References

- [1] Croucher, M. D. and Patterson, D. *J. Solution Chem.* **9**(10), 771–784 October (1980).
- [2] de Gennes, P. G. and Prost, J. *The Physics of Liquid Crystals*. Clarendon Press, Oxford, (1993).
- [3] van Roie, B., Leys, J., Denolf, K., Glorieux, C., and Pitsi, G. and Thoen, J. *Phys. Rev. E* **72**(4), 041702 October (2005).

- [4] Kowel, S., Kornreich, P., and Cleverly, D. *Appl. Opt.* **23**(2), 278–289 (1984).
- [5] Stølen, S., Grande, T., and Allan, N. *Chemical Thermodynamics of Materials: Macroscopic and Microscopic Aspects*. John Wiley & Sons, (2004).
- [6] Lansac, Y., Fried, F., and Maïssa, P. *Phys. Rev. E* **52**(6), 6227–6239 December (1995).
- [7] Cermelli, P., Fried, E., and Gurtin, M. E. *Arch. Rational Mech. Anal.* **174**(2), 151–178 November (2004).
- [8] Kramer, L. and Pesch, W. *Annu. Rev. Fluid Mech.* **27**(1), 515–539 (1995).
- [9] Penz, P. A. *Phys. Rev. Lett.* **24**(25), 1405–1409 Jun (1970).
- [10] Fried, E. *Arch. Rational Mech. Anal.* (not yet published April 2007).
- [11] Gurtin, M. E. *Zeitschrift für Angewandte Mathematik und Physik (ZAMP)* **42**(3), 370–388 May (1991).
- [12] Gurtin, M. E. and Struthers, A. *Arch. Rational Mech. Anal.* **112**(2), 97–160 June (1990).
- [13] Marinov, Y. and Simova, P. *J. Phys. D: Appl. Phys.* **25**(10), 1495–1499 (1992).
- [14] Khalifa, A. *Energy Convers. Manage.* **42**(4), 491–504 (2001).